THE JOURNAL OF PHYSICAL CHEMISTRY A

Article

Cite This: J. Phys. Chem. A 2019, 123, 11022−11030

pubs.acs.org/JPCA

A General Approach To Combine the Advantages of Collinear and Noncollinear Spectrometer Designs in Phase-Resolved Second-Order Nonlinear Spectroscopy

Tobias Garling,[†] R. Kramer Campen,[‡,†] Martin Wolf,[†] and Martin Thämer*[,†]

[†]Department of Physical Chemistry, Fritz Haber Institute of the Max Planck Society, 14195 Berlin, Germany

[‡]Faculty of Physics, University of Duisburg-Essen, Lotharstraβe 1, 47048 Duisburg, Germany

Supporting Information

ABSTRACT: Recent years have seen a huge progress in the development of phase-sensitive second-order laser spectroscopy which has proven to be a very powerful tool for the investigation of interfaces. In these techniques, the nonlinear interaction between two short laser pulses and the sample yields a signal pulse which subsequently interferes with a third pulse, the so-called local oscillator. To obtain accurate phase information, the relative phases between the signal and local oscillator pulses must be stabilized and their timings precisely controlled. Despite much progress made, fulfilling both requirements remains a formidable experimental challenge. The two common approaches employ different beam geometries which each yields its particular advantages and deficiencies. While noncollinear spectrometers allow for a relatively simple timing control they typically yield poor phase stability and require a challenging alignment. Collinear approaches in contrast come with a simplified alignment and improved phase stability but typically suffer from a highly limited timing control. In this contribution we present a general experimental solution which allows for combining the advantages of both approaches while being compatible with most of the common spectrometer types. On the basis of a collinear geometry, we exploit different selected polarization states of the light pulses in well-defined places in the spectrometer to achieve a precise timing control. The combination of this technique with a balanced detection scheme allows for the acquisition of highly accurate phase-resolved nonlinear spectra without any loss in experimental flexibility. In fact, we show that the implementation of this technique allows us to employ advanced pulse timing schemes inside the spectrometer, which can be used to suppress nonlinear background signals and extend the capabilities of our spectrometer to measure phase-resolved sum frequency spectra of interfaces in a liquid cell.

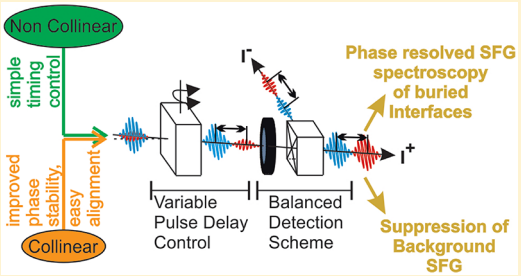

INTRODUCTION

Second-order nonlinear spectroscopies like sum frequency, difference frequency, or second harmonic generation spectroscopy (SFG, DFG, or SHG, respectively) have recently become an indispensable tool for the characterization of interfaces. Compared to their linear counterparts, these techniques offer the advantage of interface specificity (within the electric dipole approximation) provided the adjoining bulk media possess centrosymmetry. This intrinsic interface sensitivity opens up the possibility to selectively probe and characterize interfacial species and to study interfaces between bulk condensed phases. As a result of these unique properties, SFG, DFG, and SHG spectroscopies have been successfully applied to study interfacial phenomena in research areas, including medicine,[1,2] electrochemistry,[3] environmental,[4] and material sciences.[5,6]

In second-order nonlinear spectroscopies two incident laser fields E_1 and E_2 with different (SFG, DFG) or equal frequencies (SHG) are overlapped at the desired interface to generate a third field E_{sig} which is detected and analyzed. This nonlinear process is driven by the complex material response which is described by the second-order susceptibility $\chi^{(2)}$.[7−9]

$$E_{Sig} \propto \chi^{(2)} E_1 E_2 \tag{1}$$

The spectrum of $\chi^{(2)}$ reveals resonant transitions in the interfacial species at the pump and/or the signal frequencies, and the sign of its imaginary part (+ or −) is directly related to their orientation with respect to the interface.[7,10] To extract the complex $\chi^{(2)}$ spectrum in a measurement, the amplitude and phase of the generated signal field E_{Sig} must be determined. Phase-sensitive techniques typically do so by superimposing E_{Sig} with a reference beam of known phase, the so-called local oscillator (LO).[7,11] The detected heterodyned intensity I_{det} is then given by

$$I_{det} = |E_{sig} + E_{LO}|^2 \tag{2}$$

To obtain the desired phase and amplitude of the signal the quantity, E_{Sig} must be extracted from the measured intensity I_{det}. Various types of phase-sensitive nonlinear spectrometers

Received: October 22, 2019
Revised: November 25, 2019
Published: December 2, 2019

that have recently been designed follow different approaches to achieve this. They can roughly be divided into two types:[11] scanning time domain approaches (narrowband or broadband versions) and broadband multiplexed frequency domain techniques.[10,12−16] In time domain approaches the intensity modulation in I_{det} is recorded while the relative phases of E_{Sig} and E_{LO} are shifted. This can be done by scanning the relative time delay between the pulses E_{Sig} and E_{LO}[12] or by modulating the carrier envelope phase within one of the pulses. This second possibility is exploited in a recently developed broadband time domain SFG scheme.[13,17]

In the alternative broadband frequency domain approach, the local oscillator pulse is typically delayed by a few picoseconds with respect to the signal pulse leading to sharp interference fringes in the spectral domain which can be recorded by a polychromator. Through inverse Fourier filtering of $I_{det}(\omega)$ the phase and amplitude of E_{Sig} can then be determined.[15,18,19]

Apart from the aforementioned differences, all techniques rely on one common technical requirement: fine control over the relative phases between E_{Sig} and E_{LO} either for scanning the phases or for setting the pulse delays to the required values.[11,18,19] The experimental implementation of such a control is, as we show in the following, nontrivial.

The advent of laser systems delivering femtosecond pulses has led to the development of broadband spectroscopic techniques which offer crucial advantages over the ordinary narrowband approaches. Performing nonlinear spectroscopy with such pulses increases the conversion efficiency of nonlinear processes and allows for covering a large spectral range in a single experiment without the need for time-consuming frequency scans.[20] Obviously, if the two pump pulses are short (femtoseconds to picoseconds), they must be precisely overlapped in time to generate a nonlinear signal. In heterodyned second-order spectroscopy both the LO and the sample signal are typically generated consecutively by the same pump pulse pair (or a replica extracted by a beamsplitter) to ensure a well-defined phase relationship between E_{Sig} and E_{LO}.[12,14,18,19,21] The pump pulses must then be temporally overlapped at both the sample and the location of LO generation (typically a reference crystal) in the spectrometer. As shown above, it is simultaneously required that the relative time delay between the LO and the signal can be freely tuned.

The most common solution to achieve this timing control is to use a noncollinear spectrometer design (see Figure 1A).[7,10,16,22] The pump pulses have thereby different incidence angles, and the generated LO and signal waves are emitted in a third direction (determined through phase matching[9]). That way en route toward the sample the two pump pulses and the local oscillator all are spatially separated, allowing for independent control of their phases (e.g., by introducing dispersive media of various thickness in any of the beams). Though the ease of timing control in this noncollinear approach is highly beneficial, it comes with important technical and operational disadvantages. The spacial separation of the three beams between the reference and the sample position strongly reduces the phase stability of the interferometer, and the resulting phase drifts can severely distort the obtained complex spectra.[19] This phase instability can be reduced by using common optics for all beams (see Figure 1A), which in turn leads to a strong reduction in degrees of freedom for the alignment of the three beams onto the sample. In particular, obtaining a perfect spatial overlap of the incident pump beams

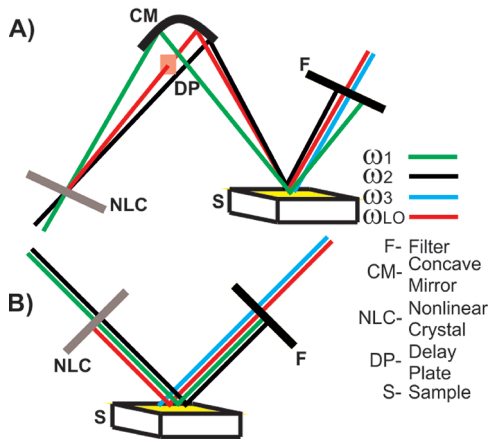

Figure 1. Common heterodyned SFG spectroscopy setups: (A) noncollinear geometry; (B) collinear geometry. ω_1 = IR, ω_2 = 800 nm, ω_3 = SFG, and ω_{LO} = local oscillator.

at both the sample position and the reference crystal while simultaneously matching the angle of the emitted signal to the reflection angle of the LO now becomes a considerable experimental obstacle. Furthermore, the phase matching direction or emission angle respectively for the signal and the LO depends in a noncollinear setup on the frequencies of the incident pulses,[9] making a repetition of the alignment procedure mandatory whenever one of the frequencies is modified. Finally, this approach causes the relative phase of the LO and the signal to be sensitive to the exact positioning of the sample, which lowers comparability of the results from different samples.

All these challenges can be circumvented by using a full collinear design (Figure 1B) which offers improved phase stability, largely simplified alignment, and high phase reproducibility upon exchange of samples.[15,23,24] However, this comes at the price of reduced flexibility to control the pulse timings. Any dispersive material that is inserted into the beam path between the reference crystal and the sample position now acts on all the three beams simultaneously. Achieving a correct setting of the different pulse timings is hardly possible with this method. A second undesired side effect of the collinear geometry is the possible generation of background nonlinear signal contributions originating from the surfaces of the beam guiding optics inside the spectrometer. Because of the collinearity, the pump beams do not exclusively overlap at the sample and reference crystal position but also at several other optical elements. Without a suitable experimental solution to this problem the resulting background contribution may be indistinguishable from the sample signal and can lead to distortion in the obtained complex spectrum. The comparison between the two spectrometer geometries seems to suggest that the choice to make use of the strength of one approach intrinsically excludes the possibility to benefit from the strengths of the other.

In this article we present a method that allows for combining the advantages of the noncollinear and the collinear spectrometer designs. The method is based on a collinear approach, and we will show how a precise timing control of the involved beams can still be achieved without any loss in experimental flexibility. Furthermore, we will demonstrate how the contributions from background signals that appear in collinear spectrometers can efficiently be suppressed.

DOI: 10.1021/acs.jpca.9b09927
J. Phys. Chem. A 2019, 123, 11022−11030

In the next section we first present the general principles and equations for the collinear timing control, followed by the result section, where we demonstrate the performance of the technique using two representative applications: the successful suppression of background signals and the measurement of the heterodyned vibrational second-order spectrum of a self-assembled monolayer inside an electrochemical cell.

CONCEPT

The key to a precise timing control between the pulses E_{Sig} and E_{LO} in a collinear beam geometry without affecting the phases of the pump pulses E_1 and E_2 is to introduce the relative time delay between the signal and the LO in the detection beam path after the sample and the reference crystal. Here the presence of the pump pulses is not required; they can thus be filtered out, and only two beams with the same frequencies, the LO and the SFG signal, remain propagating collinearly. To address the two pulses independently, they need to differ in at least one property. One possible way is to make use of their respective polarization direction. Supposing E_{Sig} and E_{LO} have orthogonal polarization, then we can shift their timing using a birefringent crystal[25] as shown in the following.

The time T any light pulse takes to travel through a bulk material depends on its frequency ω and the corresponding refractive group index $n_g(\omega)$ as well as the distance l:

$$T = \frac{n_g(\omega)l}{c} \tag{3}$$

with c being the speed of light in a vacuum. The distance l depends on the bulk thickness d, the wave's angle of refraction α', and its polarization. In the case of a uniaxial birefringent crystal, two values for l are obtained corresponding to the ordinary and extraordinary propagation inside the crystal and are given by

$$l_{o,e} = \frac{d}{\cos(\alpha'_{o,e} + \rho_{o,e})} \tag{4}$$

Here ρ is the walk-off angle which accounts for the mismatch between the Poynting and wave vector in anisotropic media. While ρ is zero for the ordinary wave, its value for the extraordinary wave can be calculated according to[26]

$$\tan(\rho) = \frac{\sin(\delta + \alpha'_e)\cos(\delta + \alpha'_e)({n_{p,o}}^2 - {n_{p,e}}^2)}{{n_{p,o}}^2 \sin^2(\delta + \alpha'_e) + {n_{p,e}}^2 \cos^2(\delta + \alpha'_e)} \tag{5}$$

In this equation $n_{p,o}$ and $n_{p,e}$ are the ordinary and extraordinary phase refractive indices, respectively, and δ the crystal cut angle as defined in Figure 2.

α' is obtained via Snell's law as a function of the incident angle α (eq 6).

$$(\alpha'_{e,o}) = \sin^{-1}\left(\frac{\sin(\alpha)}{n_{p;e,o}(\omega)}\right) \tag{6}$$

A pulse whose electric field is orthogonal to the optical axis (OA), such as the nonlinear signal, always experiences the same phase refractive index $n_{p,o}$, which is independent of the refracted angle. In contrast, a pulse whose electric field lies in the plane defined by the pulse's wave vector and the OA (e.g., the local oscillator) will experience an effective phase refractive index $n_{p,eff}$ given by[27]

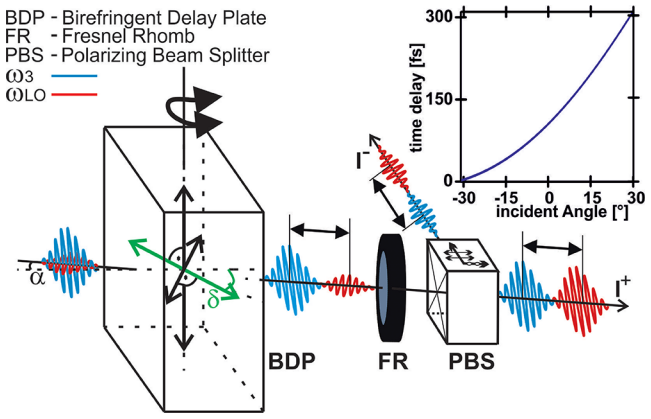

Figure 2. Working principle of the time delay compensation unit. The orthogonally polarized LO and signal pulses (red and blue, respectively) of the same frequency pass a birefringent crystal which introduces a variable time delay between the pulses which can be varied as a function of the incidence angle α. δ represents the angle between the surface normal and the optical axis (green). The Fresnel rhomb turns both beams' polarizations by 45°, and the polarizing beamsplitter projects the polarizations onto a horizontal and a vertical axis to achieve balanced detection.[13,17] The so-introduced time delay as a function of incidence angle ($d_{Calcite}$ = 1 mm, δ = 25°, and λ_{SFG} = 645 nm) is shown in the graph at the upper right corner.

$$n_{p,eff} = \frac{n_{p,o}n_{p,e}}{\sqrt{{n_{p,o}}^2 \sin^2(\delta + \alpha'_e) + {n_{p,e}}^2 \cos^2(\delta + \alpha'_e)}} \tag{7}$$

Combining eqs 6 and 7, we can calculate the effective phase index as a function of the incidence angle α. For $\delta \neq 0$ the equations need to be solved numerically.

Inserting the result into eq 6, we obtain the refractive angle α' which can be used to determine the individual transit times for the two pulses through the material (eqs 3 and 4). The effective group index required for this calculation is the material constant $n_{g,o}$ for the ordinary wave while the corresponding value for the extraordinary wave can be calculated in the same manner as the phase index, using the respective values for the ordinary and extraordinary group refractive indices $n_{g,o}$ and $n_{g,e}$:[27]

$$n_{g,eff} = \frac{n_{g,o}n_{g,e}}{\sqrt{{n_{g,o}}^2 \sin^2(\delta + \alpha'_e) + {n_{g,e}}^2 \cos^2(\delta + \alpha'_e)}} \tag{8}$$

To obtain the overall relative delay of the two pulses upon arrival at the detector, one has to finally account for the additional distance that the ordinary beam travels outside the birefringent crystal (eq 9) caused by the difference in the refracted angles between the ordinary and the extraordinary waves.[27]

$$T_{ex} = \frac{1}{c}((\tan(\alpha'_e + \rho) - \tan(\alpha'_o))d \sin\alpha) \tag{9}$$

The curve showing the overall induced time delay between the two pulses as a function of incident angle is also shown in Figure 2. The calculation was performed assuming a 1 mm thick calcite crystal with a crystal cut angle of 25° at a wavelength of 645 nm, which corresponds to our experimental parameters. The results show that such a birefringent crystal can indeed be used to smoothly vary the relative time delay between the LO and the nonlinear signal pulse over hundreds of femtoseconds. The crystal must be aligned such that the LO

DOI: 10.1021/acs.jpca.9b09927
J. Phys. Chem. A 2019, 123, 11022−11030

electric field lies either in or orthogonal to the plane defined by the wave vector and the OA. Larger delays if desired can be obtained using a thicker crystal or by modifying the crystal cut angle.

With this possibility of controlling the time delay between the signal and the LO pulse in hand, we come to the question of how the interference between the two pulses can be detected. Within our assumption the two beams are orthogonally polarized and hence do not show any interference effects if detected directly. However, they can be brought to interference by introducing a balanced detection scheme.[13,17,28] To do so, the polarizations of the two beams are each projected onto two new polarization axes which are rotated by 45°. This can be realized with a combination of a waveplate with a polarizing beamsplitter which are placed behind the birefringent crystal (see Figure 2). The resulting two beams now both contain the interference between the two pulses, however, with opposite signs as shown in eq 10 and depicted in Figure 2.[13]

$$I^- = \frac{1}{2}|E_{Sig}|^2 + \frac{1}{2}|E_{LO}|^2 - E_{Sig}E_{LO}$$
$$I^+ = \frac{1}{2}|E_{Sig}|^2 + \frac{1}{2}|E_{LO}|^2 + E_{Sig}E_{LO} \quad (10)$$

Recording the difference of the detected intensities from both resulting beams allows to isolate the pure interference term. Furthermore, the cancellation of the square terms $|E_{Sig}|^2$ and $|E_{LO}|^2$ in the difference of the detector response efficiently reduces noise that originates from intensity fluctuations, mainly from the much stronger LO. Improvements of 1 order of magnitude in signal-to-noise ratio can easily be achieved with this detection scheme.[17]

So far, we have assumed that the signal and LO waves are orthogonally polarized. To use the presented technique for second-order spectroscopy studies, we need to consider the different signal polarizations that can be generated in the sample. In such measurements the nonlinear sample signal is typically acquired as a function of the polarization combination between input and output fields with respect to the sample surface (S or P polarizations). To measure the response in a particular polarization combination (e.g., PPP) using the presented technique, the polarization of the local oscillator must be tuned to be orthogonal to the polarization of interest of the nonlinear signal (in this example to S polarization). In the case that the nonlinear sample signal is purely S or P polarized for a given set of pump beam polarizations (as is the case for most samples), we directly obtain through balanced detection the desired interference term between the LO and the nonlinear signal as shown in eqs 10. However, for samples that possess in-plane anisotropy the nonlinear signal can have contributions in both polarization directions (S and P) which give rise to two additional interference terms in eqs 10. While the interference term between the LO and the parallel polarization component of the sample signal cancels just as the square terms (interference term has equal signs for both detectors), the interference between the two polarization components of the nonlinear signal contributes to the balanced result. Although this undesired interference term is usually much smaller than the cross-term with the LO (the LO intensity is typically much larger than the sample signal), its presence can have an impact on the obtained nonlinear spectrum depending on the spectrometer type where the presented technique is implemented. The time domain SFG approach used in this contribution is based on a phase modulation between the nonlinear sample signal and the LO (see the Results section and Supporting Information) which leads to a modulation of the corresponding cross-term. The interference between two possible polarization components in the sample signal in contrast remains constant during this modulation. Consequently, its contribution does not affect the resulting spectrum. This situation is different, for example, in the case of the common broadband frequency domain SFG approach. Here, both cross-terms would contribute to the interference fringes in the spectral domain which can require their separation. One possibility to remove the undesired contribution for this spectrometer type is to simply perform a second measurement of the sample with the local oscillator blocked and to subtract the result from the previous acquisition.

In conclusion, by placing the birefringent crystal and the balanced detection scheme in series in the detection beam path, we can obtain control over the relative pulse delays and detect any polarization component of a nonlinear signal from the sample. Importantly, this holds independently from the polarization states of the pump pulses since they are no longer present in the detection beam path.

One additional important requirement for this type of detection is, however, that the LO exhibits a clean linear polarization. Furthermore, this polarization must be tunable to any polarization direction independent of the selected polarizations of the pump beams. Achieving this in a collinear beam geometry is again nontrivial because in this case the polarization of the LO cannot be controlled by placing a waveplate and a polarizer into the LO beam. One solution is to use a thin z-cut α-quartz crystal for the generation of the LO, which is placed at normal incidence into the beam path of the two collinear pump pulses before or after the sample. As a result of the noncentrosymmetric crystal structure of the α-quartz, a second-order signal is generated inside the bulk which is emitted in transmission direction and can be subsequently used as LO. Because in our collinear case all beams travel along the quartz' OA, the pulses do not experience any birefringence, and as a consequence the resulting LO pulse is perfectly linearly polarized. Furthermore, as shown in the Supporting Information, the polarization direction of the LO can be continuously tuned by simply rotating the quartz crystal about its z-axis. This property thereby holds for any combination of pump beam polarization. The use of the z-cut quartz wafer to generate the LO therefor offers precisely that degree of flexibility in polarization control which is needed.

As illustrated above, the technical solution to include all the advantages of a noncollinear beam geometry in a collinear spectrometer design contains three parts: (1) the control of the relative time delay between the LO and the signal using a birefringent crystal, (2) the balanced detection scheme to extract the interference term, and (3) LO generation with polarization control in a z-cut α-quartz crystal. There have recently been quite similar approaches published where pulse delay control is achieved by exploiting the properties of a birefringent crystal inside the spectrometer (mainly for SHG spectrometers).[29] However, the way this timing control is implemented requires a certain polarization combination between pump and signal pulses which limits the applicability of the technique to particular experimental settings. In contrast, the approach presented here is a general solution

DOI: 10.1021/acs.jpca.9b09927
J. Phys. Chem. A 2019, 123, 11022−11030

which is compatible with most of the common SHG and SFG spectrometer types (time domain as well as frequency domain techniques) without imposing any limitations on the choice of beam polarizations. Furthermore, it can be implemented in already existing homodyned second-order spectrometers quite easily to upgrade them into more powerful, collinear, and phase-sensitive heterodyned versions.

RESULTS AND DISCUSSION

After the introduction of the concept for adjusting the delay between the local oscillator (LO) and the nonlinear sample response in collinear spectrometers, we now demonstrate its experimental application. The experiments are performed using our recently developed phase-sensitive, collinear, time domain SFG spectrometer shown in Figure 3 where we implemented

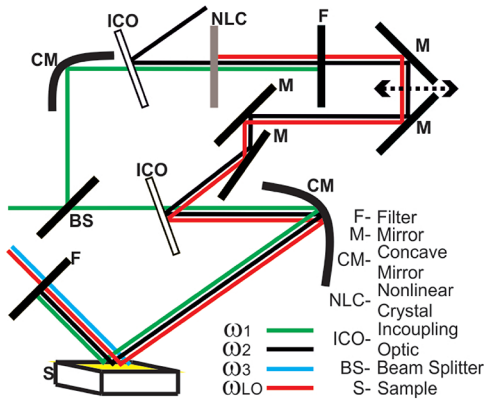

Figure 3. Schematic representation of our phase-sensitive collinear time domain SFG spectrometer. ω_1 = IR, ω_2 = 800 nm, ω_3 = SFG, and ω_{LO} = local oscillator.

the described optical setup in the detector beam path.[17] In this time domain approach the sum frequency signal and the LO pulse are generated by nonlinear mixing of two ultrashort pump pulses—one in the infrared spectral range and the other centered at 800 nm. The 800 nm beam is aligned to consecutively pass a *z*-cut quartz wafer at which the LO is generated and the sample while the beam is overlapped at these two positions with individual portions of the infrared beam in a collinear fashion (see Figure 3). The separation of the two IR portions is achieved by the use of a beamsplitter, and both partial beams are fed into the 800 nm beam path by two custom-made incoupling optics. While this splitting of the infrared pulses into two portions is a mandatory step in this time domain SFG technique, it can also be beneficial to other spectrometer types (e.g., frequency domain approaches). Above 3500 nm α-quartz shows significant absorption of infrared light which can lead to intensity losses on the way to the sample. Using two portions of the infrared light for the generation of the LO and the sample signal circumvents this problem. After filtering out the pump beams the resulting heterodyned SFG signal passes a calcite plate for pulse delay control to be finally detected by using the aforementioned balanced detection setup. An interferogram is recorded by modulating the carrier envelope phase (CEP) and amplitude of the SFG signal with respect to the CEP of the LO while the SFG signal and the LO temporally overlap to maximize the interference amplitude.[13] The CEP modulation is obtained by shifting the relative phases (changing the time delays) of the two infrared portions used to generate the LO and signal pulse, respectively. Fourier transformation of the resulting interferogram yields the complex valued SFG spectrum which is frequency resolved along the IR spectral axes. More details about the optical setup can be found in the Supporting Information and in the corresponding publications.[17,21]

Suppression of Background SFG Contributions. In a first example to demonstrate the capabilities of our technique, we turn to the problem of possible contamination of a nonlinear signal with background contributions caused by the collinear design (see the Introduction). In our spectrometer background signals can originate from the incoupling optic and the focusing parabolic mirror depicted in Figure 3. This situation is schematically shown in Figure 4A. Although these background contributions are generally small because the beams are usually not focused other than onto the sample and the reference crystal for the generation of the LO, they can become significant when samples are investigated which only yield small nonlinear signals.

Figure 4A shows a measurement of the nonresonant SFG response of a *z*-cut α-quartz sample which we use to illustrate this problem. The obtained interferogram contains the sample signal and a background SFG contribution of unknown magnitude. Without employing a suitable technique these contributions are inseparable.

One possible way of distinguishing these signals in a collinear approach is to avoid that the pulses simultaneously overlap in time at the sample and the beam guiding optics. This can be done by introducing a 3 mm thick fused silica plate at normal incidence into the beam path right before the sample (see Figure 4B). Because of group velocity dispersion (GVD) inside the material, the different pulses get temporally separated and no longer arrive at the sample simultaneously. This temporal separation of the two pump pulses leads to a suppression of the sample signal. However, the background SFG and LO experience the same delay through GVD inside the fused silica and still overlap in time at the detector and thus show an interference signal. Note that the calcite delay crystal is not installed in these cases of Figure 4A,B. The resulting interferogram is shown in Figure 4B and displays the isolated SFG background contribution. As expected, its amplitude is smaller than the nonlinear sample signal, but with a ratio of 1:10 it can easily be resolved. Considering that our sample signal originates from the relatively strong off-resonant bulk response of α-quartz the obtained size of the background contribution is indeed significant. For studies of samples that yield smaller nonlinear signals the relative size of the background contribution would be increased up to the point that it could even dominate the overall signal. This finding is remarkable since we took extensive precautions to avoid the generation of such signals during the design process of the spectrometer. Such precautions include, for example, a careful choice of the materials used for the installed optics and keeping reflection angles close to normal incidence. The presence of such background signals is therefore likely to be a common phenomenon in collinear spectrometers. In fact, phase shifts and spectral distortions originating from the interference of the sample signal with such background contributions may have contributed to the difficulties to obtain reproducible phase-resolved SFG spectra from the air−water interface which have resulted in controversial discussions.[14,30−32] It might therefore be appropriate to revisit some phase-resolved SFG studies while accounting for background signals.

DOI: 10.1021/acs.jpca.9b09927
J. Phys. Chem. A 2019, 123, 11022−11030

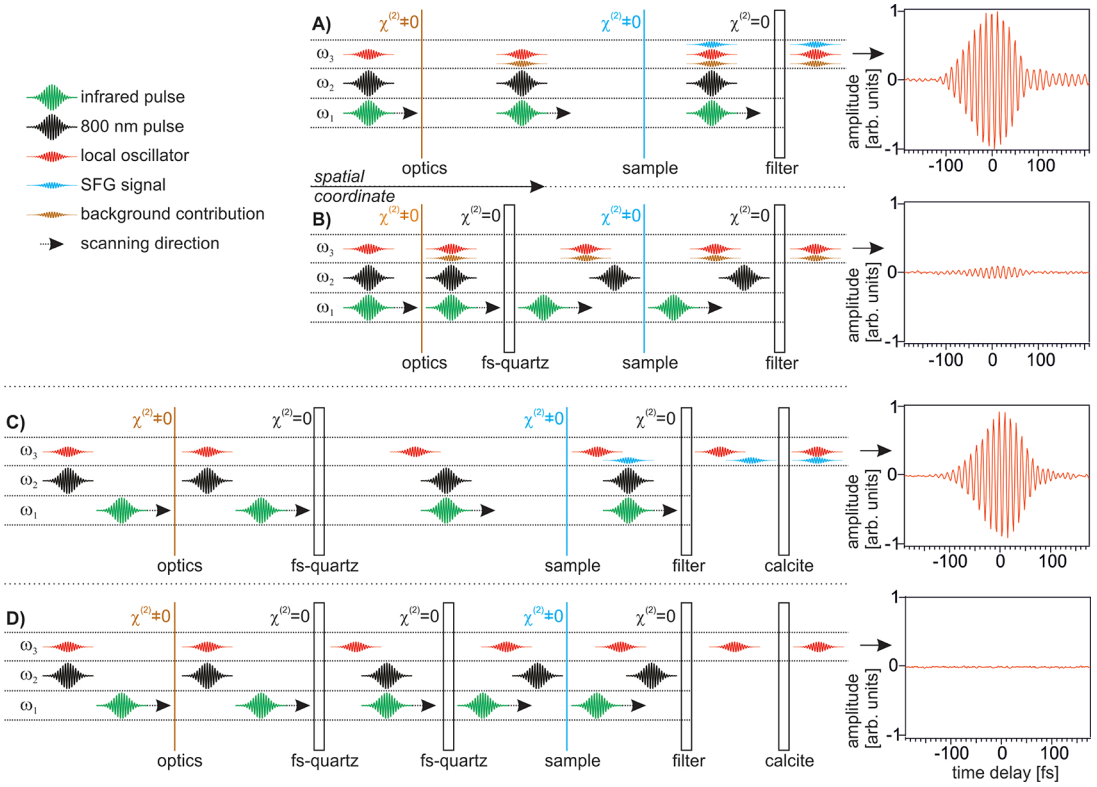

Figure 4. Analysis and suppression of background SFG contributions. (A) Common interferogram as obtained in our collinear setup, acquired under ppp polarization combination. Introduction of a quartz plate before the sample in (B) suppresses the generation of sample signal. The residual SFG originates from SFG background. In (C) the pump pulses are delayed with respect to each other to exclusively overlap in time at the sample position. The resulting timing mismatch between the LO and the sample signal is compensated by inserting and adjusting the calcite crystal. (D) Control experiment. A second femtosecond quartz plate is introduced into the beam which eliminates the sample signal. For comparability all interferograms where normalized to the one shown in (A).

Using the technique presented in Figure 4B, we can determine the amplitude and phase of the background SFG, and we could in principle subtract the resulting interferogram from the total interferogram acquired before (Figure 4A). However, it would be more convenient and certainly more accurate if the background contribution was suppressed during the sample measurement. To achieve this, we keep the previously installed fused silica plate in the beam path but move the relative pulse delays between the IR and upconversion beam such that they exclusively overlap in time at the sample position as shown in Figure 4C. Analogous to the suppression of the sample signal in Figure 4B, the result should here be a suppression of the background contribution. However, because of the GVD in the fused silica plate, the LO now lags behind the upconversion beam and hence ultimately behind the sample signal, which largely diminishes the interference amplitude. As shown in the Concept section, this timing mismatch can be compensated by inserting and tuning the calcite plate in the detection beam path. The resulting interferogram is depicted in Figure 4C and shows the desired pure sample spectrum. The amplitude of the interferogram is comparable to the measurement in Figure 4A. This confirms the successful delay compensation with the calcite plate.

The analysis of the three interferograms in Figure 4A–C is based on the assumption that the signal suppression by introducing the respective time delays is efficient and that there is no signal generated inside the fused silica window. While the latter assumption is clearly supported by theoretical considerations (see the Supporting Information), the validity of both assumptions can be tested experimentally. In this control experiment a second fused silica window is introduced into the beam path before the sample, and the settings for the initial relative pulse delays are kept the same as in Figure 4C. The schematic representation of this experiment is shown in Figure 4D. In this configuration the background and the sample SFG should both be suppressed, and according to the second assumption we do not expect any nonlinear signal from the second fused silica plate. We should thus not detect any interference signal in the experiment. The result of the measurement shown in Figure 4D is in perfect agreement with this prediction. This confirms the validity of our analysis.

The experimental settings in Figure 4C are thus an approach to obtain precise and background free SFG spectra within our spectrometer type while benefiting from its collinear design. Similar timing schemes can also be adopted for other experimental approaches such as frequency domain techniques in a straightforward manner.

Phase-Resolved SFG Measurements of Electrochemical Interfaces in a Liquid Cell. In the second application example we turn to the field of SFG studies of buried interfaces such as the electrode surface in an electrochemical cell. To gain insight into fundamental electrochemical processes that take place at the electrode–electrolyte interface, those surfaces have been extensively characterized by using homodyne vibrational SFG.[33−36] The typical goal in these studies is to identify molecular species at the interface by analyzing their vibrational resonances in a SFG spectrum. One challenge in such

DOI: 10.1021/acs.jpca.9b09927
J. Phys. Chem. A 2019, 123, 11022−11030

investigations is the presence of a nonresonant (with respect to the infrared frequencies) SFG contribution $\chi^{(2)}_{NR}$ which arises from the surface of most metal electrodes.[11,37] $\chi^{(2)}_{NR}$ exhibits a particular but often unknown phase and mixes with the resonant molecular responses $\chi^{(2)}_{R}$ (quite analogous to the background SFG in the previous example). The effective second-order susceptibility is then given by eq 11.

$$\chi^{(2)} = \chi^{(2)}_{NR} + \chi^{(2)}_{R} \tag{11}$$

Homodyned SFG techniques directly measure the spectral intensity of the emitted SFG signal: the squared modulus of the effective susceptibility. The obtained spectrum is then the frequency-dependent $|\chi^{(2)}|^2$.

$$|\chi^{(2)}|^2 = |\chi^{(2)}_{NR}|^2 + |\chi^{(2)}_{R}|^2 + 2\mathrm{Re}|\chi^{(2)}_{NR}\chi^{(2)}_{R}{}^{*}| \tag{12}$$

Problematic for the analysis of such spectra is the presence of the interference cross-term $|\chi^{(2)}_{NR}\chi^{(2)}_{R}{}^{*}|$ which can significantly alter the spectral shape of the resonant features depending on the phase and amplitude of the nonresonant contribution. The phase and amplitude of $\chi^{(2)}_{NR}$ in turn have been shown to sensitively depend on the surface potential and surface electronic structure of the electrode.[38] For potential-dependent measurements it is therefore highly nontrivial to evaluate whether observed changes in a measured homodyned SFG spectrum originate from changes in the resonant response of the interfacial molecular species caused by e.g. changes in molecular orientation or structural changes as a result of electrochemical reactions or from a change in the nonresonant response. Obtaining a correct interpretation of the observed spectral changes is without further knowledge hardly possible. Applying heterodyned vibrational SFG spectroscopy to these systems can overcome this ambiguity because the quantity $\chi^{(2)}$ is directly measured as in eq 11. This allows for separately analyzing changes in the two contributions. However, to our knowledge such measurements have so far not been realized.[11]

Performing heterodyned SFG spectroscopy on these buried liquid−solid interfaces is a very similar experiment to that shown in Figure 4C. To prevent the evaporation of the solvent, such cells are typically covered by some window material (see Figure 5A). Because all beams must pass through the window and the liquid to access the interface of interest, they experience a GVD similar to the case of introducing the fused silica plate into the beams. As for the fused silica case the resulting timing mismatch between LO and SFG signal can be compensated by tuning the calcite plate in the detection beam path.

To demonstrate the functionality of our approach for the investigation of electrochemical interfaces, we present SFG measurements of a self-assembled monolayer (SAM) of octadecanethiol (ODT) on a gold mirror. The sum frequency spectrum of the Au-ODT SAM in air is dominated in the C−H stretch region by three distinct resonance peaks from the terminal methyl groups of the molecular chain.[39] These resonant peaks can be attributed to the symmetric C−H stretch vibrations at $\nu \approx 2875$ cm^{-1} and $\nu \approx 2935$ cm^{-1} (Fermi resonance) and to the antisymmetric stretch vibration at $\nu \approx 2962$ cm^{-1}.[39] Two additional small peaks usually observed in ODT SAMs at $\nu \approx 2850$ cm^{-1} and $\nu \approx 2900$ cm^{-1} are related to gauche defects in the SAM.[39]

To mimic the experimental situation in an electrochemical cell, we enclosed the ODT-covered gold surface in a liquid cell (see Figure 5A). This cell consists of the sample and a 50 μm thin Teflon spacer covered with a calcium fluoride (CaF_2) window. The small volume between the sample and the window is filled with deuterated acetonitrile.

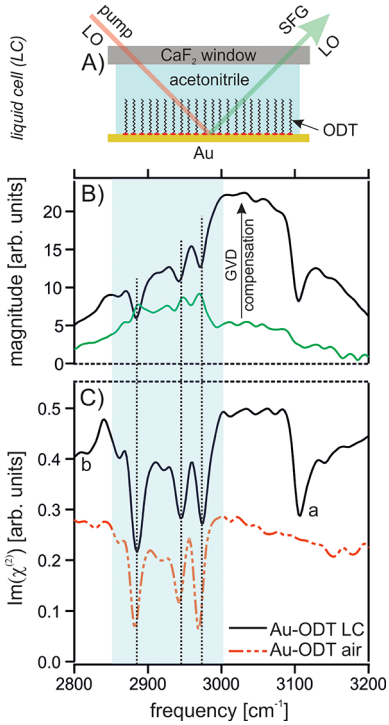

Figure 5. Phase-resolved SFG measurements of Au-ODT in a liquid cell acquired under ppp polarization combination: (A) sketch of the experimental configuration, (B) raw magnitude SFG spectra of Au-ODT under acetonitrile with (black line) and without GVD compensation (green line); (C) imaginary parts of $\chi^{(2)}$ for Au-ODT under acetonitrile (black line) and in air (red dotted line, vertically shifted for better visibility). The spectra in (C) are corrected for the spectral profile of the IR pulse. Dotted black lines indicate peak positions from the ODT response.

In a first measurement the sum frequency spectrum of the sample is acquired without compensating for the GVD in the CaF_2 window followed by the same experiment with the calcite crystal installed in the detection beam path for compensation. The resulting magnitude spectra are depicted in Figure 5B. The spectrum obtained with the GVD compensation (black line) nicely shows the three expected resonance peaks (appearing as dips) of the ODT SAM on top of a broad nonresonant background signal which originates from the Au surface. The spectrum obtained without compensation (green line), in contrast, shows a largely reduced signal intensity which is only slightly above the noise level in the spectrum. Interestingly, the relative phases between resonant and nonresonant contributions seem here to be inverted. This result clearly shows that the timing mismatch between the LO and the SFG signal leads to severe spectral distortions and confirms the necessity of the time delay compensation.

To verify whether our delay compensation technique yields an accurate spectrum, we also compare the result to a spectrum of the Au-ODT sample exposed to air where no compensation is required (see Figure 5C).

The well-ordered and dense structure of the SAM should, for steric reasons, prevent the molecules from changing their orientation or structure when in contact with the liquid. We thus expect that the nonlinear spectral responses of the ODT

DOI: 10.1021/acs.jpca.9b09927
J. Phys. Chem. A 2019, 123, 11022−11030

monolayer are similar in both experiments. Figure 5C shows the imaginary (absorptive) part of the second-order susceptibility for the Au-ODT sample which are extracted from the measurements in the liquid cell (black line) and in air (red dotted line). Comparing the line shapes of the three resonance peaks from the ODT layer shows indeed a very close match between the two spectra. The most prominent differences appear in the spectrum from the liquid cell in regions outside the frequency window of the ODT resonances. They are labeled a and b (onset of a negative peak) in Figure 5C. Because these peaks also appear in a control experiment of the same cell without ODT (not shown in this contribution), they must originate from molecular species which are introduced with the solvent. However, deuterated acetonitrile does not show significant bulk absorption peaks in the measured region. The exact origin of the peaks is unknown, but they likely originate either from impurities in the solvent which accumulate at the gold surface or from solvent related formation of interfacial species which interact with the gold layer. While a more detailed investigation of the origin of peaks a and b is beyond the scope of this contribution, the comparison to the Au-ODT spectrum in air indicates that the phase-resolved spectrum measured in the liquid cell is indeed accurate.

Furthermore, this example shows more generally how our timing control technique enables us to extent the capabilities of our collinear spectrometer e.g. to SFG studies on electrodes in electrochemical cells.

SUMMARY

We have presented an experimental method that allows for precise timing control between the local oscillator and the nonlinear signal in collinear spectrometers for second-order nonlinear spectroscopy. By exploiting the polarization-dependent group delay in a birefringent crystal in combination with a polarization-based balanced detection scheme, this technique yields continuous tunability of the relative pulse delay without imposing any particular requirements on the polarizations of pump pulses or the detected sample signal. The presented solution for the timing control is very general and can readily be implemented in most of the common spectrometer types including time domain and frequency domain approaches. That way it is possible to benefit from the superior phase accuracy and a simplified spectrometer alignment of a collinear design while maintaining full experimental flexibility.

The applicability of this technique goes beyond simple measurements of nonlinear spectra in a collinear spectrometer. As demonstrated in the Results section, we can use the ability to control the pulse delay to freely modify the pulse sequences in different places inside the spectrometer. We have shown that this can be used to either isolate or suppress the nonlinear background contributions which originate from the beam steering optics inside the optical setup. Our results indicate that such background signals can indeed have a significant size in collinear setups which potentially results in falsified nonlinear sample spectra. The presented suppression method is therefore an essential ingredient to ensure high accuracy in the nonlinear spectra obtained with a collinear approach.

Furthermore, we have demonstrated how the technique extends the capabilities of our time domain SFG spectrometer to measure phase-resolved spectra of buried interfaces which are enclosed in a liquid cell. These types of measurements will be further pursued to investigate the fundamental processes at electrochemical interfaces.

ASSOCIATED CONTENT

Supporting Information

The Supporting Information is available free of charge at https://pubs.acs.org/doi/10.1021/acs.jpca.9b09927.

Details on experimental setup, comments on the polarization control of the local oscillator, discussion on possible nonlinear signals from fused silica (PDF)

AUTHOR INFORMATION

Corresponding Author

*E-mail: thaemer@fhi-berlin.mpg.de.

ORCID

Martin Thämer: 0000-0002-9631-9280

Notes

The authors declare no competing financial interest.

ACKNOWLEDGMENTS

This study was supported by the European Research Council (ERC) under the European Union's Horizon 2020 research and innovation program (Grant 772286 to R.K.C.).

REFERENCES

(1) Fu, L.; Wang, Z.; Batista, V. S.; Yan, E. C. New Insights from Sum Frequency Generation Vibrational Spectroscopy into the Interactions of Islet Amyloid Polypeptides with Lipid Membranes. *J. Diabetes Res.* **2016**, *2016*, 1.

(2) Fu, L.; Wang, Z.; Yan, E. C. Chiral Vibrational Structures of Proteins at Interfaces Probed by Sum Frequency Generation Spectroscopy. *Int. J. Mol. Sci.* **2011**, *12*, 9404−9425.

(3) Zwaschka, G.; Wolf, M.; Campen, R. K.; Tong, Y. A Microscopic Model of the Electrochemical Vibrational Stark Effect: Understanding VSF Spectroscopy of (bi)Sulfate on Pt(111). *Surf. Sci.* **2018**, *678*, 78−85.

(4) Jubb, A. M.; Hua, W.; Allen, H. C. Organization of Water and Atmospherically Relevant Ions and Solutes: Vibrational Sum Frequency Spectroscopy at the Vapor/Liquid and Liquid/Solid Interfaces. *Acc. Chem. Res.* **2012**, *45*, 110−119.

(5) Humbert, C.; Noblet, T.; Dalstein, L.; Busson, B.; Barbillon, G. Sum-Frequency Generation Spectroscopy of Plasmonic Nanomaterials: A Review. *Materials* **2019**, *12*, 836.

(6) Tegeder, P. Optically and Thermally Induced Molecular Switching Processes at Metal Surfaces. *J. Phys.: Condens. Matter* **2012**, *24*, 394001.

(7) Stiopkin, I. V.; Jayathilake, H. D.; Bordenyuk, A. N.; Benderskii, A. V. Heterodyne-Detected Vibrational Sum Frequency Generation Spectroscopy. *J. Am. Chem. Soc.* **2008**, *130*, 2271−2275.

(8) Shen, Y. R. Surfaces Probed by Nonlinear Optics. *Surf. Sci.* **1994**, *299*, 551−562.

(9) Lambert, A. G.; Davies, P. B.; Neivandt, D. J. Implementing the Theory of Sum Frequency Generation Vibrational Spectroscopy: A Tutorial Review. *Appl. Spectrosc. Rev.* **2005**, *40*, 103−145.

(10) Nihonyanagi, S.; Yamaguchi, S.; Tahara, T. Direct Evidence for Orientational Flip-Flop of Water Molecules at Charged Interfaces: A Heterodyne-Detected Vibrational Sum Frequency Generation Study. *J. Chem. Phys.* **2009**, *130*, 204704.

(11) Shen, Y. R. *Fundamentals of Sum-Frequency Spectroscopy*; Cambridge University Press: 2016.

(12) Pettinger, B.; Bilger, C. A Novel Approach to Analyze the Optical Second Harmonic Generation Anisotropy at Surfaces Employing Interference Techniques. Example: the Au(110) Electrode. *Chem. Phys. Lett.* **1998**, *286*, 355−360.

DOI: 10.1021/acs.jpca.9b09927
J. Phys. Chem. A 2019, 123, 11022−11030

(13) Laaser, J. E.; Xiong, W.; Zanni, M. T. Time-Domain SFG Spectroscopy Using Mid-IR Pulse Shaping: Practical and Intrinsic Advantages. *J. Phys. Chem. B* **2011**, *115*, 2536−2546.
(14) Sun, S.; Liang, R.; Xu, X.; Zhu, H.; Shen, Y. R.; Tian, C. Phase Reference in Phase-Sensitive Sum-Frequency Vibrational Spectroscopy. *J. Chem. Phys.* **2016**, *144*, 244711.
(15) Xu, B.; Wu, Y.; Sun, D.; Dai, H.-L.; Rao, Y. Stabilized Phase Detection of Heterodyne Sum Frequency Generation for Interfacial Studies. *Opt. Lett.* **2015**, *40*, 4472.
(16) Vanselous, H.; Petersen, P. B. Extending the Capabilities of Heterodyne-Detected Sum-Frequency Generation Spectroscopy: Probing Any Interface in Any Polarization Combination. *J. Phys. Chem. C* **2016**, *120*, 8175−8184.
(17) Thämer, M.; Campen, R. K.; Wolf, M. Detecting Weak Signals from Interfaces by High Accuracy Phase-Resolved SFG Spectroscopy. *Phys. Chem. Chem. Phys.* **2018**, *20*, 25875−25882.
(18) Nihonyanagi, S.; Mondal, J. A.; Yamaguchi, S.; Tahara, T. Structure and Dynamics of Interfacial Water Studied by Heterodyne-Detected Vibrational Sum-Frequency Generation. *Annu. Rev. Phys. Chem.* **2013**, *64*, 579−603.
(19) Shen, Y. Phase-Sensitive Sum-Frequency Spectroscopy. *Annu. Rev. Phys. Chem.* **2013**, *64*, 129−150.
(20) Richter, L. J.; Petralli-Mallow, T. P.; Stephenson, J. C. Vibrationally Resolved Sum-Frequency Generation with Broad-Bandwidth Infrared Pulses. *Opt. Lett.* **1998**, *23*, 1594−1596.
(21) Thämer, M.; Garling, T.; Campen, R. K.; Wolf, M. Quantitative Determination of the Nonlinear Bulk and Surface Response from alpha-Quartz Using Phase Sensitive SFG Spectroscopy. *J. Chem. Phys.* **2019**, *151*, No. 064707.
(22) Yamaguchi, S.; Tahara, T. Heterodyne-Detected Electronic Sum Frequency Generation: "Up" versus "Down" Alignment of Interfacial Molecules. *J. Chem. Phys.* **2008**, *129*, 101102.
(23) Ji, N.; Ostroverkhov, V.; Chen, C.-Y.; Shen, Y.-R. Phase-Sensitive Sum-Frequency Vibrational Spectroscopy and Its Application to Studies of Interfacial Alkyl Chains. *J. Am. Chem. Soc.* **2007**, *129*, 10056−10057.
(24) Wang, H.; Gao, T.; Xiong, W. Self-Phase-Stabilized Heterodyne Vibrational Sum Frequency Generation Microscopy. *ACS Photonics* **2017**, *4*, 1839−1845.
(25) Wilson, J. W.; Bartels, R. A. Rapid Birefringent Delay Scanning for Coherent Multiphoton Impulsive Raman Pump−Probe Spectroscopy. *IEEE J. Sel. Top. Quantum Electron.* **2012**, *18*, 130−139.
(26) Guenther, B. D. *Modern Optics* ; Oxford University Press: 2015.
(27) Schlup, P.; Wilson, J.; Hartinger, K.; Bartels, R. A. Dispersion Balancing of Variable-Delay Monolithic Pulse Splitters. *Appl. Opt.* **2007**, *46*, 5967−5973.
(28) Jones, K. C.; Ganim, Z.; Tokmakoff, A. Heterodyne-Detected Dispersed Vibrational Echo Spectroscopy. *J. Phys. Chem. A* **2009**, *113*, 14060−14066.
(29) Ohno, P. E.; Chang, H.; Spencer, A. P.; Liu, Y.; Boamah, M. D.; Wang, H.-f.; Geiger, F. M. Beyond the Gouy−Chapman Model with Heterodyne-Detected Second Harmonic Generation. *J. Phys. Chem. Lett.* **2019**, *10*, 2328−2334.
(30) Nihonyanagi, S.; Ishiyama, T.; Lee, T.-k.; Yamaguchi, S.; Bonn, M.; Morita, A.; Tahara, T. Unified Molecular View of the Air/Water Interface Based on Experimental and Theoretical $x^{(2)}$ Spectra of an Isotopically Diluted Water Surface. *J. Am. Chem. Soc.* **2011**, *133*, 16875−16880.
(31) Nihonyanagi, S.; Kusaka, R.; Inoue, K.; Adhikari, A.; Yamaguchi, S.; Tahara, T. Accurate Determination of Complex $x^{(2)}$ Spectrum of the Air/Water Interface. *J. Chem. Phys.* **2015**, *143*, 124707.
(32) Tian, C.-S.; Shen, Y. R. Isotopic Dilution Study of the Water/Vapor Interface by Phase-Sensitive Sum-Frequency Vibrational Spectroscopy. *J. Am. Chem. Soc.* **2009**, *131*, 2790−2791.
(33) Tong, Y.; Lapointe, F.; Thämer, M.; Wolf, M.; Campen, R. K. Hydrophobic Water Probed Experimentally at the Gold Electrode/Aqueous Interface. *Angew. Chem., Int. Ed.* **2017**, *56*, 4211−4214.
(34) Baldelli, S.; Markovic, N.; Ross, P.; Shen, Y.-R.; Somorjai, G. Sum Frequency Generation of CO on (111) and Polycrystalline Platinum Electrode Surfaces: Evidence for SFG Invisible Surface CO. *J. Phys. Chem. B* **1999**, *103*, 8920−8925.
(35) Wang, J.; Xu, M.; Huangfu, Z.; Wang, Y.; He, Y.; Guo, W.; Wang, Z. Observation of Gold Electrode Surface Response to the Adsorption and Oxidation of Thiocyanate in Acidic Electrolyte with Broadband Sum-Frequency Generation Spectroscopy. *Vib. Spectrosc.* **2016**, *85*, 122−127.
(36) Tadjeddine, A.; Guyot-Sionnest, P. Spectroscopic Investigation of Adsorbed Cyanide and Thiocyanate on Platinum Using Sum Frequency Generation. *Electrochim. Acta* **1991**, *36*, 1849−1854.
(37) Vidal, F.; Tadjeddine, A. Sum-Frequency Generation Spectroscopy of Interfaces. *Rep. Prog. Phys.* **2005**, *68*, 1095−1127.
(38) Bilger, C.; Pettinger, B. Potential Dependence of the Non-Linear Polarizability of an Au (110) Electrode. *J. Chem. Soc., Faraday Trans.* **1998**, *94*, 2795−2801.
(39) Potterton, E.; Bain, C. Infrared-Infrared Sum-Frequency Generation from Adsorbates on Metal Surfaces. *J. Electroanal. Chem.* **1996**, *409*, 109−114.

DOI: 10.1021/acs.jpca.9b09927
J. Phys. Chem. A 2019, 123, 11022−11030